Electron Momentum Distribution of Terbium by Compton Scattering Technique

B. L. Ahuja, H. Malhotra, and M. Sharma

Department of Physics, College of Science, M. L. Sukhadia University,
Udaipur - 313001 (Rajasthan) India.

Reprint requests to Dr. B. L. A.; E-mail: blahuja@yahoo.com

We present the experimental Compton profile of polycrystalline terbium, using 661.65 keV gamma-rays, emitted by 20 Ci ^{137}Cs. In the absence of band structure calculations, theoretical computations have been made using renormalised-free-atom (RFA) and free electron based profiles. It is seen that the RFA results with e^--e^- correlation correction agree relatively better with the experiment. The data are interpreted in terms of spd-f hybridization in the valence state of terbium. From the RFA profile, we have also derived the cohesive energy of terbium, which is compared with other band structures and experimental investigations. – PACs Nos. 13.60.F, 71.15.Nc, 78.70. -g, 78.70.Ck

Key words: Compton Profile; Electron Momentum Density; Electron-electron Correlation Effects; Cohesive Energy; Rare-earth Metals.

1. Introduction

Terbium (Tb) crystals have the hcp structure (lattice parameters $a = 3.606$ Å and $c = 5.697$ Å). The 4f electrons of the lanthanides are very different from the s, p and d valence electrons of other atoms. They bear great resemblance to core electrons. Due to this interesting behavior, considerable work has been done on them, which includes the energy position of the 4f levels, the valence states and their stability, band structure calculations of full potential linearized augmented plane waves (FLAPW) and linear muffin tin orbitals (LMTO) etc., see for example [1 – 10]. Compton scattering, which is inelastic scattering of X-rays, can be utilized to probe the ground states electronic properties [11]. The Compton profile $J(p_z)$ is the projection of the scatterers electron momentum density $\rho(\boldsymbol{p})$ along the scattering vector $\boldsymbol{k}$ generally, chosen as the Z-axis:

$$J(p_z) = \int\limits_{p_x} \int\limits_{p_y} \rho(\boldsymbol{p}_x, \boldsymbol{p}_y, \boldsymbol{p}_z) \mathrm{d}p_x \mathrm{d}p_y. \qquad (1)$$

In case of isotropic systems, (1) is usually rewritten in terms of the radial momentum distribution. Since $\rho(\boldsymbol{p}_x, \boldsymbol{p}_y, \boldsymbol{p}_z)$ is the probability distribution of the Compton profile, the normalization rule $\int_{-\infty}^{\infty} J(p_z)\mathrm{d}p_z = N$ follows, where N is the total number of the scattering electrons. The Compton line shape is very sensitive to the behavior of the valence electrons, and offers a straight forward way to compare the band structure calculations of different materials.

There are some advantages if photons with high incident energies can be used to probe the electronic structure of rare earth elements, in which the binding energy of the K shell electrons is of the order of 50 keV. Therefore, scattering from the K shell cannot be treated within the impulse approximation, when a low incident energy (like 60 keV from ^{241}Am) is used.

In our endeavour to extend the Compton profile studies of rare-earth elements [12, 13], in the current paper we present first an isotropic Compton profile of Tb, using our 20 Ci ^{137}Cs Compton spectrometer. Due to the non-availability of a theoretical directional Compton profile and difficulties (like the requirement of ultra high vacuum conditions and the chemical reactivity of rare-earths) in growing large single crystals (say 15 mm dia. and 5 mm thickness), we have decided to measure the first isotropic Compton profile of Tb. The renormalised-free-atom (RFA) model is known to be a reasonable compromise between an elaborate band structure and a simple atomic calculations. In the absence of band structure calculations based on Compton profiles, we have also interpreted

our results in terms of RFA Compton profiles computed by us. We have also corrected our RFA data for the e^--e^- correlation effect. To check the feasibility of the Compton data in reproducing the cohesive energy of rare earths, we have also derived for the first time the cohesive energy of Tb from the RFA Compton data and compared it with other available experimental and theoretical data.

2. Experiment

Many Compton profile measurements have been made using a low energy gamma-ray source (like ^{241}Am) in conjunction with an HPGe detector. These measurements are hampered by their low momentum resolution. In our experiment a 20 Ci ^{137}Cs source is used, because its low photoelectric absorption, long half life and large energy transfer makes it particularly suitable for Compton profile studies. A description of the experimental set-up alongwith the Compton profile of liquid Hg is given in [14]. The high purity (99.9+%) Tb sample was a polycrystalline sheet of 12 mm × 12 mm × 0.4 mm. The incident beam of 661.65 keV gamma-rays was scattered by the sample through a mean angle of $160° \pm 0.6°$. The energy spectrum of the scattered radiation was measured with a Ge detector (Canberra, Model GL0210P, resolution 630 eV at 188.5 keV, the position of the Compton peak). In momentum scale, this detector had a corresponding resolution of 0.365 a. u. (Gaussian FWHM). The divergence of the incident and scattered beams was determined using a Monte Carlo simulation, and an additional resolution broadening 0.153 a. u. was found, leading to an overall momentum resolution as 0.40 a. u. (Gaussian FWHM). During the measurement, the stability of the system was checked from time to time using weak ^{57}Co and ^{133}Ba gamma-ray calibrators. An integrated Compton intensity of $1.5 \cdot 10^7$ photons was obtained after 319 hours exposure of the sample. The background was measured with the sample removed. After the background correction, the raw data were placed on the energy scale and corrected for energy dependent corrections like instrumental resolution, detector efficiency, absorption correction, scattering cross-section, etc. using a well tested scheme of the Warwick group [15]. An objective of the correction due to instrumental resolution was to remove the effects produced by the detector response tail from the measured data, leaving the profile with a resolution of 0.4 a. u. (Gaussian FWHM). Finally, the experimental profile was cor-
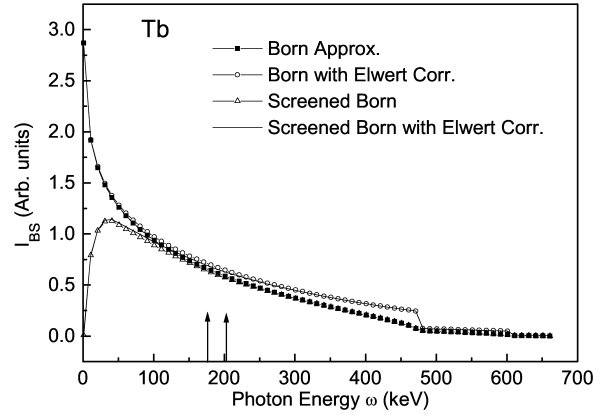

Fig. 1. Spectrum of the bremsstrahlung intensity of Tb Born approximation, and with and without Elwert factor and screening corrections. Two vertical arrows show the Compton region which corresponds to -7 a. u. to $+7$ a. u. For details we refer to [14] and section II of this paper.

rected for the effects of multiple photon-electron scattering. A Monte Carlo procedure [16] was used to calculate the momentum distribution of the multiple scattered gamma-rays. The contribution of the multiple scattering, which was found to be 4.2% in the momentum region 0 to +10 a. u., was subtracted from the measured profile. After application of data processing routines the high energy side of the profile was normalized to the free atom profile [17] in the momentum range 0 to 7 a. u. In addition to the above mentioned usual data analysis we have incorporated an additional correction, namely bremsstrahlung (BS) background correction, which is due to the continuous spectrum of BS emitted by photo and Compton electrons. The detailed procedure of the BS correction has already been reported in [14]. For the BS correction we have calculated the differential BS cross-section (within the relativistic Born approximation) for the emission of photons with energy ω, as mentioned in [14]. In addition to our earlier prescription [14], we have corrected the BS intensity I_{BS} for the Elwert correction and screening effects, as suggested by Seltzer and Berger [18]. The spectral distribution of BS calculated for the decelerating electrons liberated in photoelectric and Compton processes from 661.65 keV γ-rays in Tb is shown in Figure 1. The intensity ratio $I_{BS}^{CP}/I_{BS}^{Total}$ (intensity of BS in the Compton region relative to the total BS intensity), which is calculated from the BS intensity curve incorporating the Elwert factor and screening effects, as shown in Fig. 1, comes out to be 0.05815. The intensity ratio $I_{BS}^{Total}/I_{C}^{Total}$, where I_{C}^{Total} is the total inten-

sity of Compton electrons, is calculated using the relations [19]

$$I_{BS}^{Total} = N(w_0)kZ[\sigma_c(w_0, Z)(w_0 - w_c)^2$$
$$+ \sum_i \sigma_{p,i}(w_0, Z)(w_0 - E_B^i)^2], \quad (2)$$

$$I_C^{Total} = N(w_0)\sigma_c(w_0, Z)w_c. \quad (3)$$

Here $N(\omega_0)$ is the incident flux of photons with energy w_0, E_B^i is the binding energy of the ith shell of the target element, σ corresponds to respective cross-section, w_c is the average energy of the Compton scattered photons, which in our case is about 189 keV (Compton peak) and the constant k is $7 \cdot 10^{-7} keV^{-1}$.

The product of these two ratios, which corresponds to I_{BS}^{CP}/I_C^{Total}, comes out to be 0.0052. The I_{BS}^{CP}/I_C^{Total} ratio was then multiplied by 49.30 electrons, viz the number of electrons participating in the Compton scattering phenomenon in the momentum range -7.0 a. u. to $+7.0$ a. u. to get the data of the BS profile (in e/a.u.). This number (0.26 e^- in the present case) was used to normalise the area under the 'screened Born with Elwert corrected' BS curve in the Compton region (-7 a. u. to $+7$ a. u.), as shown of Figure 1. The resulting profile corresponds to an additional BS background, which was subtracted from the earlier-corrected profile point by point. The BS corrected profile was again normalised to the total area of the free atom profile in the momentum range 0 to $+7$ a. u.

3. Calculations

Since the theoretical Compton profiles the from band structure calculations for Tb were not available, we have computed the Compton profile using the RFA model [20, 21], which was applied successfully in earlier studies on 3d, 4d and 5d transition metals, see, for example [14, 22 – 25]. The procedure is briefly described here. Other details are skipped, as they are available in [20, 21]. The Hartree-Fock wave functions for the outermost 6s electrons were taken from the table of Fischer [26]. These free atom wave functions were terminated at the Wigner-Seitz (WS) radius and renormalised to one, to preserve charge neutrality. It turned out that only 29.8% of the atomic 6s electron wave function was inside the WS sphere. In the RFA model, the momentum density per atom, associated for the 6s band of a hcp crystal, can be given as

$$\rho(p) = 2 \sum_{|p - K_n| \le p_F} |\psi_0^c(K)|^2 [1 + \cos K_n \tau]/2, \quad (4)$$

where $\psi_0^c(K)$ is the Fourier transform (FT) of the RFA wave function $\psi_0^c(r)$; K_n is a reciprocal lattice vector for the nth shell. p_F is the Fermi momentum and τ determines the position of an atom in the unit cell. To incorporate the crystalline effects, altogether the contribution of 25 reciprocal lattice vectors was considered.

In addition to the RFA calculation, we have also calculated free electron model based Compton profile of Tb. The free electron theory serves for metals in most cases as a first approximation. Using free electron theory, the Compton profile for 6s electrons can be given as

$$J/(p_z) = \frac{3n}{4p_F^3}(p_F^2 - p_z^2) \quad \text{for } p_z \le p_F,$$
$$0 \qquad \qquad \text{otherwise.} \quad (5)$$

Here n is the number of free electrons per site and $p_F = (3\pi^2 n_e)^{1/3}$, where n_e is the valence electron density. Using (5), we have also calculated the free electron Compton profile for $6s^2$ electrons of Tb.

In case of both models, to get an absolute profile of the electronic configuration [Xe] $4f^9 5d^0 6s^2$ (in the momentum range 0 to 7 a. u.), the Compton profiles for core and 4f electrons were directly taken from the tables of Biggs et al. [17]. It is worth mentioning here that the inclusion of the e^--e^- correlation decreases the momentum density below the Fermi momentum and increases it above Fermi momentum. To incorporate the e^--e^- correlation correction, we have adopted the prescription of Das and Chaddah [27], which was found to be very successful in our earlier studies on Mg metal [28].

4. Results and Discussion

4.1. (i) Comparison of Compton Profiles

The experimental Compton profile of Tb, together with unconvoluted theoretical Compton profiles derived from the RFA model (with and without incorporating the e^--e^- correlation effects) and the free electron model are listed in Table 1. It is worthwhile to mention here that for a proper comparison with the theoretical data, the latter have to be convoluted with the instrumental function of the experiment. Figure 2 shows the difference profiles (ΔJ) between the convoluted theory and the experiment for different calculations. It can be seen from this figure that the free electron model based profile gives a very poor
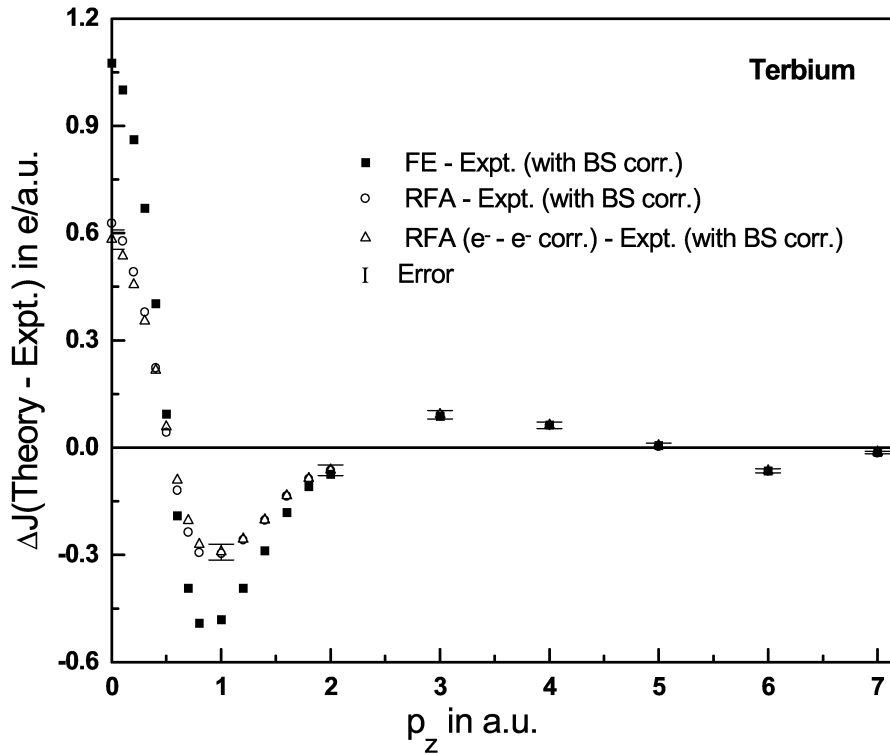
Fig. 2. Plot of differences between the experiment (BS corrected) and theoretical calculations for (a) free electron model (b) RFA model and (c) RFA with e⁻-e⁻ correlation correction.

Table 1. The theoretical (unconvoluted) and experimental Compton profiles of terbium. The experiment after bremsstrahlung (BS) background correction is shown in column 6. The statistical errors ($\pm\sigma$) are also shown at a few points.

p_z (in a. u.)	$J(p_z)$ in e/a.u.				
	FE	RFA	RFA (e⁻-e⁻)	Experiment	Experiment (with BS corr.)
0.00	10.228	9.767	9.721	9.021±0.027	9.055
0.10	10.194	9.733	9.687	8.958	8.987
0.20	9.945	9.538	9.493	8.841	8.874
0.30	9.600	9.233	9.194	8.676	8.708
0.40	9.080	8.879	8.857	8.468	8.498
0.50	8.419	8.297	8.309	8.216	8.245
0.60	7.595	7.837	7.910	7.925	7.952
0.70	6.987	7.238	7.309	7.603	7.629
0.80	6.700	6.934	6.945	7.264	7.288
1.00	6.098	6.289	6.289	6.586±0.022	6.606
1.20	5.552	5.691	5.691	5.954	5.970
1.40	5.075	5.160	5.160	5.385	5.397
1.60	4.698	4.739	4.739	4.898	4.908
1.80	4.403	4.420	4.420	4.526	4.533
2.00	4.175	4.186	4.186	4.253±0.015	4.259
3.00	3.266	3.269	3.269	3.174±0.012	3.176
4.00	2.419	2.418	2.418	2.362±0.009	2.358
5.00	1.770	1.770	1.770	1.774±0.007	1.766
6.00	1.350	1.350	1.350	1.426±0.006	1.417
7.00	1.080	1.080	1.080	1.120±0.004	1.109

agreement with the experiment, which may be due to unrealistic assumptions of free electron theory. The RFA model profile for the configuration [Xe]4f⁹5d⁰6s² with the e⁻-e⁻ correlation gives better agreement with the experiment, although in the low momentum region the RFA calculations (with and without e⁻-e⁻ correlation) give higher values than the experiment. This may be due to spd-f hybridization in the solid state phase of the Tb. It can be understood in terms of the shape of the Compton profile of different shells. Compton profiles corresponding to 6p or 5d electrons of Tb are expected to be flatter than those of 6s electrons. Hence the incorporation of 6p or 5d electrons in theoretical calculations will decreases the total theoretical profile in the vicinity of $p_z = 0$. Hence, it will lead to a better agreement between RFA calculations and the experiment. Unfortunately, 6p or 5d electron wave functions or Compton profiles are not available, therefore it is not possible to consider in detail the presence of 6p and 5d electrons in the valence band of Tb in its bulk state. The overall picture obtained is consistent with the previous LMTO calculations of Lundin et al. [9], where a better agreement between theory and experiment is obtained when including, ad-hoc, the 4f state as valence electrons even though part of these 4f states are treated as occupied core states. This is also supported by the first principles electronic structure calculations

Table 2. Cohesive energy (E_{coh}) of Tb alongwith the results of other investigators.

Reference	E_{coh} (in eV)
(a) Our RFA	4.17
(b) LMTO [7] (i) GGA	4.36
(ii) LDA	4.98
(c) Interpolation [1]	4.00
(d) Experiment [30]	4.13

of Strange et al. [8], who splitted the 4f band into two sub-bands and predicted that the f bands hybridize with the s-d bands, which straddled the Fermi energy.

4.2. (ii) Cohesive Energy

Since the operator of the kinetic energy (KE) is $p^2/2$, the study of the KE is closely related to the study of the momentum distribution. For a set of electrons, the expected value of KE is

$$T = \iiint \frac{p^2}{2} \rho(\boldsymbol{p}) \mathrm{d}p. \tag{6}$$

The cohesive energy E_{coh} is defined as the difference between the total ground-state energy of the solid state and the energy of the individual isolated atoms. The cohesive energy from the Compton profile data [29] is given as

$$E_{coh} = \int_0^{\rho_{max}} p_z^2 [J^S(p_z) - J^{FA}(p_z)] \mathrm{d}p_z, \tag{7}$$

where the $J^S(p_z)$ and $J^{FA}(p_z)$ refer to solid and free atom profiles, respectively. In our calculations, the values of J^S were taken from the present RFA calculation, and those for J^{FA} from the free atom Compton profile tables [17]. In the integral of (7) we have taken $p_{max} = 4.0$ a. u. In fact, any choice of $p_{max} > 3.0$ a. u. is justified, because after this value both the RFA and free atom profiles are the same. In Table 2, we present the cohesive energy derived from our RFA calculations together with the values obtained by other workers using

the local density approximation (LDA) and generalized gradient approximation (GGA) within the full potential LMTO [7], interpolation technique [1] and the experimental data [30]. Good agreement between our RFA based E_{coh} and the experimental data [30] is found. The fact that the RFA model does not accurately calculate the Compton profile, yet calculates reasonably the cohesive energy has been observed in our earlier work on W metal also [31]. It is already discussed by Holt and Cooper [29] and Mittal et al. [31] that the computation of cohesive energy from the experimental Compton profile is a difficult task because the weighting of p^2 in (7) in the high momentum tail magnifies the systematic errors. The calculation of cohesive energy from the experimental Compton profile and the errors in the calculation mainly depend upon the precise range over which the free atom profile may be taken to agree with the experimental profile. This matter still needs more investigations and will be reported in due time along with the a systematic trend of various rare earths.

5. Conclusions

In this paper, experimental isotropic Compton profiles of Tb have been presented and interpreted in terms of renormalised-free-atom (RFA) and free-electron based theories. The deviation between experiment and RFA theory in the low momentum region indicates hybridization of 5d and 6p electrons with the 4f electrons in the solid phase of Tb. The RFA based cohesive energy agrees with the available experimental data. Poor agreement between the RFA model and the present experiment clearly points towards the need for computation of Compton profiles using band structure methods.

[1] M. S. S. Brooks and B. Johansson, J. Phy. F: Met. Phys. **13**, l97 (1983); Also B. Johansson and A. Rosengren, Phys. Rev. B **11**, 1367 (1975).

[2] B. Johansson and P. Munck, J. Less-common Met. **100**, 49 (1984).

[3] D. J. Singh, Phys. Rev. B **44**, 7451 (1991).

[4] R. Ahuja, S. Auluck, B. Johansson, and M. S. S. Brooks, Phys. Rev. B **50**, 5147 (1994).

[5] A. Delin, L. Fast, B. Johansson, J. M. Wills, and O. Eriksson, Phys. Rev. Lett. **79**, 4637 (1997).

[6] A. Delin, L. Fast, B. Johansson, O. Eriksson, and J. M. Wills, Phys. Rev. B **58**, 4345 (1998).

[7] A. Delin, L. Fast, O. Eriksson, and B. Johansson, J. Alloys and Compounds **275 – 277**, 472 (1998).

[8] P. Strange, A. Svane, W. M. Temmerman, Z. Szotek, and H. Winter, Nature London **399**, 756 (1999).

[9] U. Lundin, I. Sandalov, O. Eriksson, and B. Johansson, Solid State Commun. **115**, 7 (2000).

[10] L. Petit, A. Svane, Z. Szotek, P. Strange, H. Winter, and W. M. Temmerman, J. Phys.: Condens. Matter **13**, 8697 (2001).

[11] M. J. Cooper, Rep. Prog. Phys. **48**, 415 (1985) and references therein.

[12] B. L. Ahuja and M. Sharma, Phys. Stat. Sol. **b 241**, 2975 (2004).

[13] B. L. Ahuja, H. Malhotra, and M. Sharma, Indian J. Phys. A (2004), in press.

[14] B. L. Ahuja, M. Sharma, and S. Mathur, Z. Naturforsch. **59a**, 543 (2004).

[15] See, for example, D. N. Timms, Ph. D. Thesis (unpublished), University of Warwick, England 1989; Also B. G. Williams, Compton Scattering McGraw-Hill, New York 1977.

[16] J. Felsteiner, P. Pattison, and M. J. Cooper, Phil. Mag. **30**, 537 (1974).

[17] F. Biggs, L. B. Mendelsohn, and J. B. Mann, Atomic Data and Nuclear Data Tables **16**, 201 (1975).

[18] S. M. Seltzer and M. J. Berger, Nucl. Instr. Meth. B **12**, 95 (1985).

[19] R. D. Evans, The Atomic Nucleus, Tata McGraw-Hill, New Delhi 1979.

[20] K. F. Berggren, S. Manninen, and T. Paakkari, Phys. Rev. B **8**, 2516 (1973).

[21] B. L. Ahuja, B. K. Sharma, and O. Aikala, Pramana-J. Phys. **29**, 313 (1986).

[22] B. K. Sharma and B. L. Ahuja, Phys. Rev. B **38**, 3148 (1988).

[23] S. Perkkio, B. K. Sharma, S. Manninen, T. Paakkari and B. L. Ahuja, Phys. Stat. Sol. (b) **168**, 657 (1991).

[24] C. Chang, S. Lee, and C. Chen, J. Physical Soc. Japan **60**, 4253 (1991).

[25] R. K. Pandya, K. B. Joshi, Rajesh Jain, B. L. Ahuja, and B. K. Sharma, Phys. Stat. Sol. (b) **200**, 137 (1997).

[26] C. F. Fischer, Atomic Data **4**, 301 (1972).

[27] G. P. Das and P. Chaddah, Solid State Comm. **45**, 607 (1983).

[28] B. L. Ahuja and B. K. Sharma, Phys. Lett. A **123**, 475 (1987).

[29] R. S. Holt and M. J. Cooper, Philos. Mag. B **41**, 117 (1980).

[30] L. J. Nugent, J. L. Burnett, and L. R. Morss, J. Chem. Thermodyn. **5**, 665 (1973).

[31] U. Mittal, B. K. Sharma, F. M. Mohammad, and B. L. Ahuja, Phys. Rev. B **38**, 12208 (1988).